

## FAR-FIELD RECONSTRUCTION FROM A MINIMUM NUMBER OF SPHERICAL SPIRAL DATA USING EFFECTIVE ANTENNA MODELINGS

F. D'Agostino, F. Ferrara, C. Gennarelli\*, R. Guerriero, and M. Migliozzi

Dipartimento di Ingegneria Elettronica ed Ingegneria Informatica, University of Salerno, via Ponte Don Melillo, Fisciano, Salerno 84084, Italy

**Abstract**—Two probe-compensated near-field-far-field transformations with spherical spiral scanning tailored for antennas having two of their dimensions very different from the third one are developed by properly applying the unified theory of spiral scans for nonspherical antennas. One is suitable for electrically long antennas, which are considered as enclosed in a cylinder ended in two half-spheres. The other adopts a surface formed by two circular “bowls” with the same aperture diameter but different lateral bends to shape a quasi-planar antenna. These flexible modelings fit very well many actual antennas by properly setting their geometric parameters. Great reduction of the number of data to be acquired is achieved, thus significantly reducing the required measurement time. Numerical tests validating the accuracy of the proposed techniques and their stability with respect to random errors affecting the data are shown.

### 1. INTRODUCTION

The near-field-far-field (NF-FF) transformation technique with spherical spiral scanning (Fig. 1), like the classical spherical one, gives the full antenna pattern coverage, even though the data processing is considerably more complex than the one needed by planar and cylindrical NF facilities [1, 2]. Unlike the spherical scanning, the spherical spiral one enables strong reduction of the time it takes to collect the NF data and this is a very important

---

*Received 27 July 2011, Accepted 28 November 2011, Scheduled 4 December 2011*

\* Corresponding author: Claudio Gennarelli (gennar@diie.unisa.it).

issue for the antenna measurements community, since nowadays the measurement time is much larger than the one needed to perform the NF-FF transformations. Such a reduction is accomplished, as suggested in [3], by employing continuous and synchronized movements of the positioning systems of the probe and antenna under test (AUT). Accordingly, NF-FF transformations using innovative spherical spiral scanings have been recently developed [4–7]. They are based on nonredundant sampling representations of electromagnetic (EM) fields [8] and use appropriate optimal sampling interpolation (OSI) formulas to reconstruct the NF data needed by the NF-FF transformation with spherical scanning [9] from the nonredundant samples acquired on the spiral. In particular, the nonredundant sampling representation on the spiral and the related two-dimensional OSI expansion have been developed by assuming the AUT enclosed in the smallest sphere able to contain it [4–6] and choosing the spiral step equal to the corresponding sample spacing needed to interpolate the data along a meridian. Unfortunately, when dealing with “nonspherical” antennas having two of their dimensions very different from the third one, the spherical AUT modeling induces a redundancy which gives rise to an useless increase in the number of the NF data to be acquired [7]. To overcome this drawback, two effective NF-FF transformations with spherical spiral scanning tailored to these kinds of antennas have been developed in [7] by properly applying the unified theory of spiral scanings for nonspherical antennas [10]. In particular, a prolate ellipsoidal modeling has been adopted when dealing with elongated antennas, whereas an oblate ellipsoidal one has been employed to model quasi-planar ones.

The goal of this contribution is to develop even more effective NF-FF transformations with spherical spiral scanning tailored to nonspherical antennas and based on highly flexible modelings, which allow one to further reduce the number of the NF data to be acquired (and the related measurement time) since they are able to better fit the shape of many antennas by properly choosing their geometric parameters. In particular, a rounded cylinder, namely a cylinder ended in two half-spheres, will be adopted in the following to model an electrically long antenna, whereas a quasi-planar one will be considered as enclosed inside a double bowl, i.e., a surface formed by two circular bowls with same aperture diameter but different lateral bends.

Note that, unlike as done in [7], where for simplicity an ideal probe was assumed, the effects of the measurement probe are properly taken into account here so that the developed NF-FF transformations are probe-compensated.

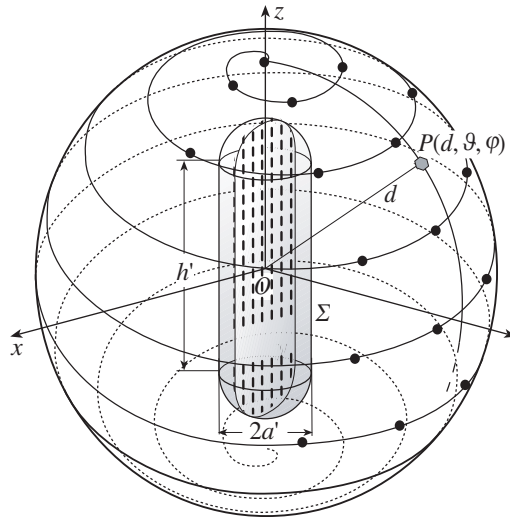


**Figure 1.** Spherical spiral scanning for an elongated antenna.

## 2. NONREDUNDANT REPRESENTATION OF THE PROBE VOLTAGE ON A SPHERE FROM SAMPLES COLLECTED ALONG A SPIRAL

Let us consider an AUT and a nondirective probe moving along a spiral wrapping a sphere of radius  $d$  in the NF region and adopt the spherical coordinate system  $(r, \vartheta, \varphi)$  for denoting an observation point  $P$  (Fig. 1). Since the voltage  $V$  measured by a nondirective probe has the same effective spatial bandwidth as the field, the theoretical results relevant to the nonredundant sampling representation of EM fields [8] can be applied. Accordingly, by assuming the AUT as enclosed in a proper rotational surface  $\Sigma$  bounding a convex domain and by describing the spiral by means of a proper analytical parameterization  $\underline{r} = \underline{r}(\eta)$ , the probe “reduced voltage”.

$$\tilde{V}(\eta) = V(\eta)e^{j\psi(\eta)}, \tag{1}$$

$\psi(\eta)$  being a phase function to be determined, can be closely approximated by a spatially bandlimited function [11]. The corresponding bandlimitation error becomes negligible as the bandwidth exceeds a critical value  $W_\eta$  [8], so that it can be effectively controlled by choosing a bandwidth equal to  $\chi' W_\eta$ , where  $\chi'$  is an excess bandwidth factor, slightly greater than unity for electrically large antennas.

The unified theory of spiral scanings for nonspherical antennas [10], obtained by paralleling the rigorous procedure [6] valid when

adopting the spherical AUT modeling, allows one to develop the voltage representation on the sphere from a nonredundant number of its samples collected along the spiral. To this end, it is necessary: i) to determine a nonredundant representation along the spiral; ii) to choose the step of the spiral such that it intersects any meridian at properly spaced points. In particular, according to [10], the bandwidth  $W_\eta$  and parameterization  $\eta$  relevant to a meridian, and the corresponding phase function  $\psi$  are given by

$$W_\eta = \beta \ell' / 2\pi \quad (2)$$

$$\eta = \frac{\pi}{\ell'} [R_1 - R_2 + s'_1 + s'_2] \quad (3)$$

$$\psi = \frac{\beta}{2} [R_1 + R_2 + s'_1 - s'_2] \quad (4)$$

where  $\beta$  is the wavenumber,  $\ell'$  is the length of the intersection curve  $C'$  between the meridian plane through the observation point  $P$  and  $\Sigma$ ,  $s'_{1,2}$  are the arclength coordinates of the two tangency points  $P_{1,2}$  between the cone of vertex at  $P$  and  $C'$ , and  $R_{1,2}$  the distances from  $P$  to  $P_{1,2}$ .

According to [10], the spiral can be got by projecting onto the scanning sphere a proper spiral wrapping  $\Sigma$ , whose step is equal to the sample spacing  $\Delta\eta = 2\pi/(2N'' + 1)$  needed to interpolate the voltage along a meridian. Note that  $N'' = \text{Int}(\chi N') + 1$ , where  $N' = \text{Int}(\chi' W_\eta) + 1$ ,  $\chi > 1$  is an oversampling factor [8] which allows the control of the truncation error, and  $\text{Int}(x)$  denotes the integer part of  $x$ . The projection is obtained via the curves at  $\eta = \text{const}$ . Therefore, the equations of the spiral are:

$$\begin{cases} x = d \sin \theta(\eta) \cos \phi \\ y = d \sin \theta(\eta) \sin \phi \\ z = d \cos \theta(\eta) \end{cases} \quad (5)$$

where  $\phi$  is the parameter describing it and  $\eta = k\phi = \phi/(2N'' + 1)$ . It is worthwhile to note that the spiral angle  $\theta$ , unlike the zenithal angle  $\vartheta$ , can take negative values.

The unified theory [10] also allows the determination of the parameter  $\xi$  and phase factor  $\gamma$  to get a nonredundant representation along the spiral. In particular,  $\gamma$  coincides with the phase function  $\psi$  relevant to a meridian, and  $\xi$  is  $\beta/W_\xi$  times the arclength of the projecting point that lies on the spiral wrapping  $\Sigma$ . Moreover,  $W_\xi$  is chosen equal to  $\beta/\pi$  times the length of the spiral wrapping the surface  $\Sigma$  from pole to pole.

In light of the above results, the reduced voltage at any point  $Q$

of the scanning spiral can be recovered via the OSI expansion [10]:

$$\tilde{V}(\xi) = \sum_{m=m_0-p+1}^{m_0+p} \tilde{V}(\xi_m) \Omega_M(\xi - \xi_m) D_{M''}(\xi - \xi_m) \quad (6)$$

where  $2p$  is the number of retained samples  $\tilde{V}(\xi_m)$ ,  $m_0 = \text{Int}(\xi/\Delta\xi)$  the index of the sample nearest (on the left) to  $Q$ , and

$$\xi_m = m\Delta\xi = 2\pi m/(2M'' + 1) \quad (7)$$

with  $M'' = \text{Int}(\chi M') + 1$  and  $M' = \text{Int}(\chi' W_\xi) + 1$ . Moreover,

$$D_{M''}(\xi) = \frac{\sin((2M'' + 1)\xi/2)}{(2M'' + 1) \sin(\xi/2)} \quad (8)$$

$$\Omega_M(\xi) = \frac{T_M \left[ -1 + 2 (\cos(\xi/2) / \cos(\bar{\xi}/2))^2 \right]}{T_M \left[ -1 + 2 / \cos^2(\bar{\xi}/2) \right]} \quad (9)$$

are the Dirichlet and Tschebyscheff Sampling functions, wherein  $T_M(\xi)$  is the Tschebyscheff polynomial of degree  $M = M'' - M'$  and  $\bar{\xi} = p\Delta\xi$ . It must be stressed that, when interpolating the voltage in the neighbourhood of the poles ( $\vartheta = 0$  and  $\vartheta = \pi$ ), it is necessary to increase the excess bandwidth factor  $\chi'$  to avoid a significant growth of the bandlimitation error in these zones [4–7].

The OSI formula (6) can be used to get the “intermediate samples”, i.e., the voltages at the intersection points between the spiral and the meridian passing through  $P$ . Once they have been evaluated, the voltage at  $P$  can be recovered via the following OSI expansion:

$$\tilde{V}(\eta(\vartheta), \varphi) = \sum_{n=n_0-q+1}^{n_0+q} \tilde{V}(\eta_n) \Omega_N(\eta - \eta_n) D_{N''}(\eta - \eta_n) \quad (10)$$

where  $N = N'' - N'$ ,  $n_0 = \text{Int}[(\eta - \eta_0)/\Delta\eta]$ ,  $2q$  is the number of the retained intermediate samples  $\tilde{V}(\eta_n)$ ,

$$\eta_n = \eta_n(\varphi) = k\varphi + n\Delta\eta = \eta_0 + n\Delta\eta \quad (11)$$

and the other symbols have the same or analogous meaning as in (6). It is then possible to recover the NF data needed to perform the spherical NF-FF transformation [9], as modified in [12, 13].

### 3. ELONGATED ANTENNAS CASE

A very flexible modeling to deal with an electrically long antenna is obtained by considering the surface  $\Sigma$  as formed by a cylinder of height

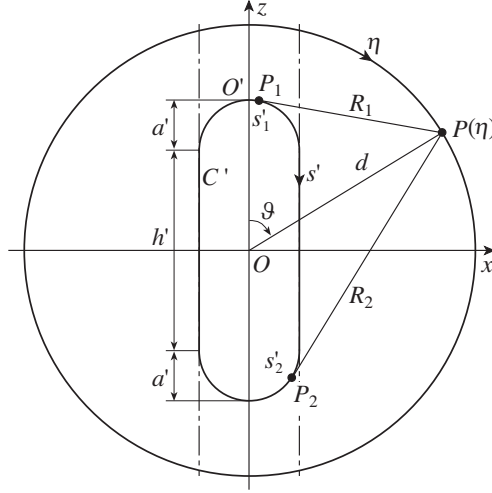


**Figure 2.** Rounded cylinder modeling.

$h'$  ended in two half-spheres of radius  $a'$  (Figs. 1 and 2). In such a way, it is possible to very well fit many real antennas by properly choosing the values of the parameters  $h'$  and  $a'$ . The expressions of the bandwidth  $W_\eta$  and parameterization  $\eta$  relevant to a meridian, and the corresponding phase function  $\psi$ , can be obtained by the general ones (2)–(4) by properly taking into account the geometry of the surface  $\Sigma$  (Fig. 2). It can be easily verified that, in such a case, the length of the intersection curve  $C'$  is  $\ell' = 2(h' + \pi a')$ , whereas the expressions of  $R_{1,2}$  and  $s'_{1,2}$  change depending on the position of the tangency points  $P_{1,2}$ . As a consequence, for  $\vartheta$  ranging in  $[0, \pi]$ , three cases must be considered (see Fig. 2):

$$1) \quad 0 \leq \vartheta \leq \sin^{-1}(a'/d)$$

$$R_1 = \sqrt{(d \sin \vartheta)^2 + (d \cos \vartheta - h'/2)^2 - a'^2} \quad (12)$$

$$s'_1 = a' \sin^{-1} \left( \frac{a'd \sin \vartheta + R_1 (h'/2 - d \cos \vartheta)}{R_1^2 + a'^2} \right) \quad (13)$$

$$R_2 = R_1 \quad ; \quad s'_2 = a' \sin^{-1} \left( \frac{a'd \sin \vartheta - R_2 (h'/2 - d \cos \vartheta)}{R_2^2 + a'^2} \right) \quad (14)$$

$$2) \quad \sin^{-1}(a'/d) < \vartheta \leq \pi - \sin^{-1}(a'/d)$$

$R_1$  and  $s'_1$  are given by (12) and (13)

$$R_2 = \sqrt{(d \sin \vartheta)^2 + (d \cos \vartheta + h'/2)^2 - a'^2} \tag{15}$$

$$s'_2 = h' + a' \left[ \pi - \sin^{-1} \left( \frac{a'd \sin \vartheta + R_2 (h'/2 + d \cos \vartheta)}{R_2^2 + a'^2} \right) \right] \tag{16}$$

3)  $\pi - \sin^{-1}(a'/d) < \vartheta \leq \pi$   
 $R_2$  and  $s'_2$  are given by (15) and (16),

$$R_1 = \sqrt{(d \sin \vartheta)^2 + (d \cos \vartheta + h'/2)^2 - a'^2} \tag{17}$$

$$s'_1 = h' + a' \left[ \frac{\pi}{2} - \sin^{-1} \left( \frac{R_1 d \sin \vartheta + a' (h'/2 + d \cos \vartheta)}{R_1^2 + a'^2} \right) \right] \tag{18}$$

The spiral and the expressions of the parameter  $\xi$  for describing it and the related phase factor  $\gamma$ , can be determined according to the unified theory of spiral scans. In particular, the spiral is obtained by projecting the one wrapping the surface  $\Sigma$  on the sphere via the curves at  $\eta = \text{const}$ , displayed in Fig. 3 with those at  $\psi = \text{const}$ .

The following simulations refer to a spiral wrapping a sphere of radius  $d = 35\lambda$  and to a uniform planar array of elementary Huygens sources polarized along the  $z$  axis, spaced by  $0.5\lambda$  ( $\lambda$  being the wavelength). These sources cover a zone in the plane  $y = 0$ , formed by a rectangle ended in two half-circles. The sizes of the rectangle are:  $2a' = 10\lambda$  and  $h' = 36\lambda$ . An open-ended circular waveguide,

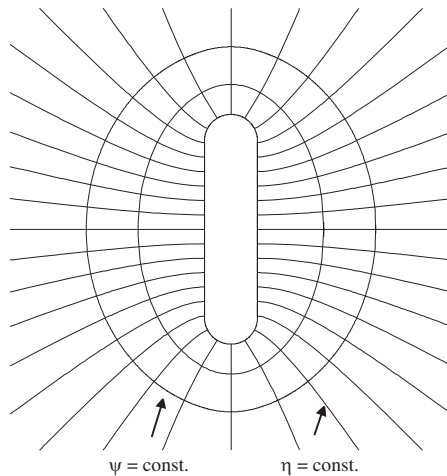


**Figure 3.** Rounded cylinder modeling: Curves  $\psi = \text{const}$  and  $\eta = \text{const}$ .

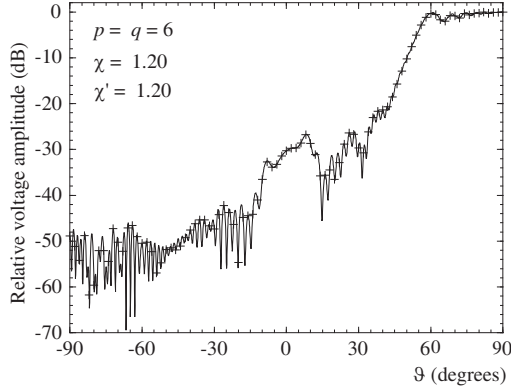


**Figure 4.** Amplitude of  $V'$  on the meridian at  $\varphi = 90^\circ$ . Solid line: Exact. Crosses: Interpolated.

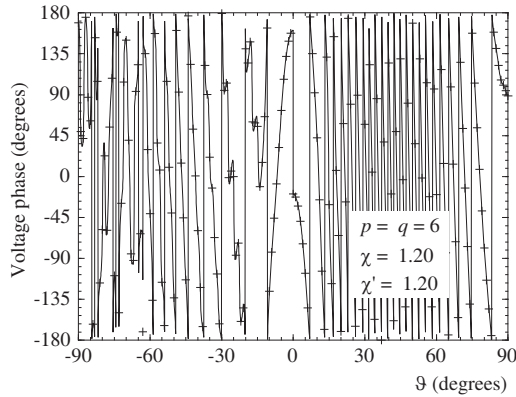


**Figure 5.** Phase of  $V'$  on the meridian at  $\varphi = 90^\circ$ . Solid line: Exact. Crosses: Interpolated.

with radius  $\rho' = 0.338 \lambda$ , is considered as measurement probe. Figs. 4 and 5 show the reconstruction of the amplitude and phase of the rotated probe voltage  $V'$  on the meridian at  $\varphi = 90^\circ$ . As can be seen, there is an excellent agreement between the exact voltage and the reconstructed one. It is useful to note that we have adopted, in the zones of the spiral determined by the 40 samples around the poles, an excess bandwidth factor such that the sample spacing is reduced exactly by a factor 7. The accuracy in the interpolation process is also confirmed by the values of the mean-square errors (normalized to the voltage maximum value on the sphere) reported in Fig. 6 for

$p = q$  ranging from 3 to 10,  $\chi' = 1.20$  (save for the polar zones), and  $\chi = 1.10, 1.15, 1.20, 1.25$ . As expected, they decrease to very low values on increasing the oversampling factor and/or the number of retained samples. The algorithm robustness has been verified by adding random errors to the exact samples. These errors simulate a background noise (bounded to  $\Delta a$  in amplitude and with arbitrary phase) and an uncertainty on the samples of  $\pm\Delta a_r$  in amplitude and  $\pm\Delta\alpha$  in phase. As shown in Fig. 7, the algorithm works well also in presence of error affected data.

At last, the developed interpolation algorithm has been applied to retrieve the NF data required to carry out the spherical NF-FF

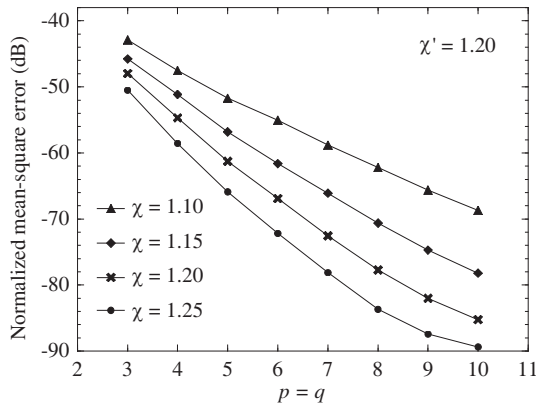


Figure 6. Normalized mean-square errors in the reconstruction of  $V'$ .

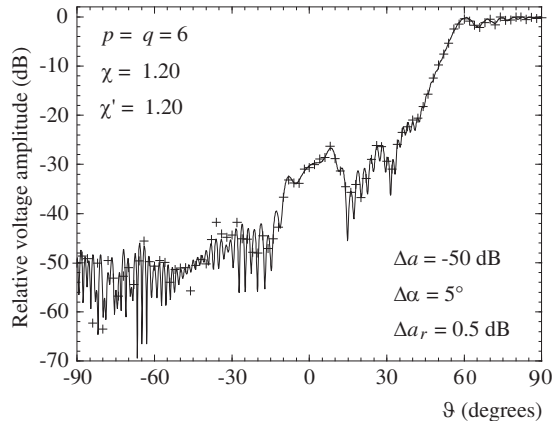
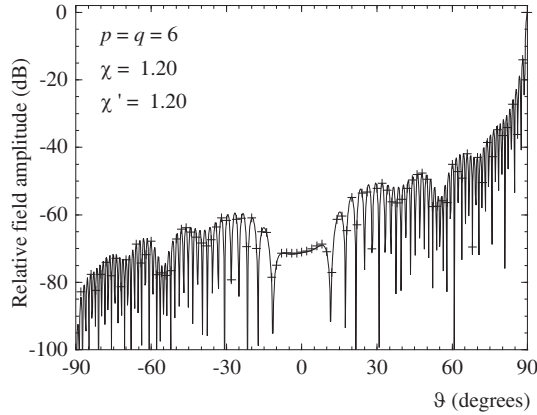
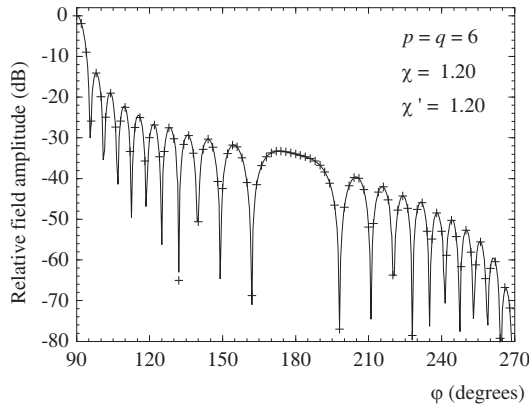


Figure 7. Amplitude of  $V'$  on the meridian at  $\varphi = 90^\circ$ . Solid line: Exact. Crosses: Interpolated from error affected data.



**Figure 8.** *E*-plane pattern. Solid line: Exact. Crosses: Reconstructed from NF measurements.



**Figure 9.** *H*-plane pattern. Solid line: exact. Crosses: Reconstructed from NF measurements.

transformation [9], as modified in [12, 13]. The reconstructions of the antenna FF pattern in the principal planes are shown in Figs. 8 and 9. As can be seen, the reconstructions are very accurate. Note that the number of samples on the spiral is 14 162, remarkably less than the one (57 550) required by the approach proposed in [6]. In particular, the number of “regular samples” at spacing  $\Delta\xi$  is 13 202, whereas the number of “extra samples” at reduced spacing is 960. Moreover, the number of samples collected along the spiral results to be much less than that (130 562) needed by the classical NF-FF transformation with spherical scanning [9].

#### 4. QUASI-PLANAR ANTENNAS CASE

When dealing with antennas which exhibit a quasi-planar geometry, a very flexible modeling can be obtained by considering them as enclosed by a surface  $\Sigma$  formed by two circular “bowls” with the same aperture diameter  $2a$ , (Figs. 10 and 11). It is worth noting that their lateral surfaces have not the same bend because they are generally determined by rotating two different circular arcs, each equal to a quarter of circumference (with radius  $c$  and  $c'$ ). This model allows a very good fitting of many antennas by properly setting the values of the parameters  $c$ ,  $c'$  and  $a$ . As a matter of fact,  $\Sigma$  coincides with a sphere if  $c = c' = a$ , it becomes a half-sphere if  $c = 0$  and  $c' = a$ , and it reduces to a circular dish for  $c = c' = 0$ .

The expressions of the bandwidth  $W_\eta$  and parameterization  $\eta$  relevant to a meridian, and the related phase function  $\psi$ , can be obtained by the general ones (2)–(4) by properly taking into account the geometry of the surface  $\Sigma$  (Fig. 11). The length of the curve  $C'$  becomes  $\ell' = 2[(a - c) + (a - c') + (c + c')\pi/2]$ . As before, the expressions of  $R_{1,2}$  and  $s'_{1,2}$  change depending on the location of the tangency points  $P_{1,2}$ , but now five cases must be considered (see Fig. 11) for  $\vartheta$  ranging in  $[0, \pi]$ :

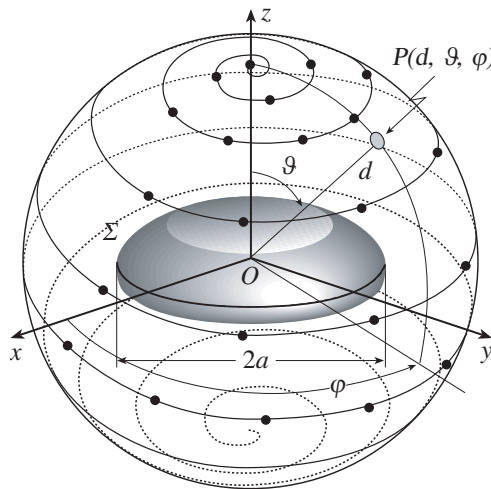


**Figure 10.** Spherical spiral scanning for a quasi-planar antenna.

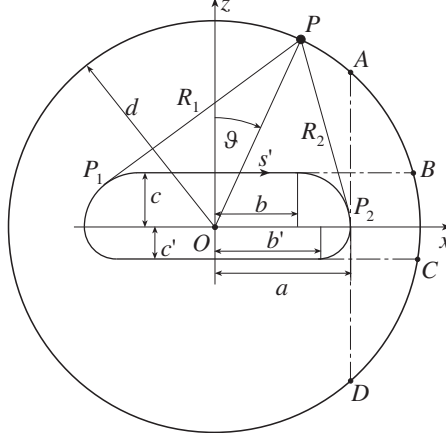


**Figure 11.** Double bowl modeling.

$$1) 0 \leq \vartheta \leq \vartheta_A = \sin^{-1}(a/d)$$

$$R_1 = \sqrt{d^2 + b^2 + 2bd \sin \vartheta - c^2}; \quad s'_1 = -(b + c\alpha_1) \quad (19)$$

$$\alpha_1 = \tan^{-1}(R_1/c) - \tan^{-1}[(b + d \sin \vartheta)/d \cos \vartheta] \quad (20)$$

$$R_2 = \sqrt{d^2 + b^2 - 2bd \sin \vartheta - c^2}; \quad s'_2 = b + c\alpha_2 \quad (21)$$

$$\alpha_2 = \tan^{-1}(R_2/c) - \tan^{-1}[(b - d \sin \vartheta)/d \cos \vartheta] \quad (22)$$

$$2) \vartheta_A < \vartheta \leq \vartheta_B = \cos^{-1}(c/d)$$

$R_1$ ,  $s'_1$ , and  $\alpha_1$  are given by (19) and (20)

$$R_2 = \sqrt{d^2 + b'^2 - 2b'd \sin \vartheta - c'^2}; \quad s'_2 = b + c(\pi/2) + c'\alpha_2 \quad (23)$$

$$\alpha_2 = \tan^{-1}(R_2/c') - \tan^{-1}[d \cos \vartheta / (d \sin \vartheta - b')] \quad (24)$$

$$3) \vartheta_B < \vartheta \leq \vartheta_C = \pi - \cos^{-1}(c'/d)$$

$R_2$ ,  $s'_2$ , and  $\alpha_2$  are given by (23) and (24)

$$R_1 = \sqrt{d^2 + b^2 - 2bd \sin \vartheta - c^2}; \quad s'_1 = b + c(\alpha_1 + \pi/2) \quad (25)$$

$$\alpha_1 = -\tan^{-1}(R_1/c) - \tan^{-1}[d \cos \vartheta / (d \sin \vartheta - b)] \quad (26)$$

$$4) \vartheta_C < \vartheta \leq \vartheta_D = \pi - \sin^{-1}(a/d)$$

$R_1$ ,  $s'_1$ , and  $\alpha_1$  are given by (25) and (26)

$$R_2 = \sqrt{d^2 + b'^2 + 2b'd \sin \vartheta - c'^2}; \quad s'_2 = b + 2b' + (c + c')(\pi/2) + c'\alpha_2 \quad (27)$$

$$\alpha_2 = \tan^{-1}(R_2/c') - \tan^{-1}[(d \sin \vartheta + b')/|d \cos \vartheta|] \quad (28)$$

$$5) \vartheta_D < \vartheta \leq \pi$$

$R_2$ ,  $s'_2$ , and  $\alpha_2$  are given by (27) and (28)

$$R_1 = \sqrt{d^2 + b'^2 - 2b'd \sin \vartheta - c'^2}; \quad s'_1 = b + c(\pi/2) + c'(\pi/2 - \alpha_1) \quad (29)$$

$$\alpha_1 = \tan^{-1}(R_1/c') - \tan^{-1}[(b' - d \sin \vartheta)/|d \cos \vartheta|] \quad (30)$$

The scanning spiral, the parameter  $\xi$  for describing it, and the corresponding phase factor  $\gamma$  are then determined according to the unified theory of spiral scannings.

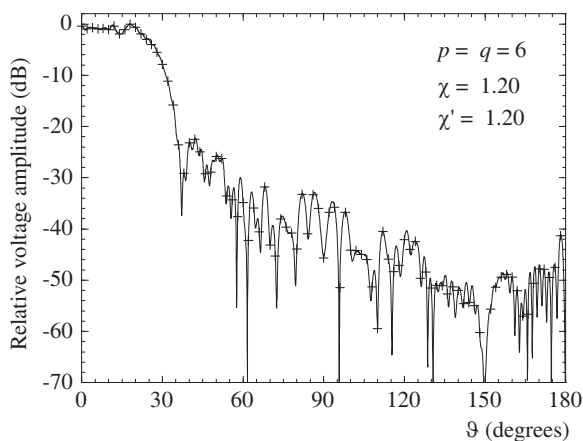


**Figure 12.** Amplitude of  $V$  on the meridian at  $\varphi = 0^\circ$ . Solid line: Exact. Crosses: Interpolated.

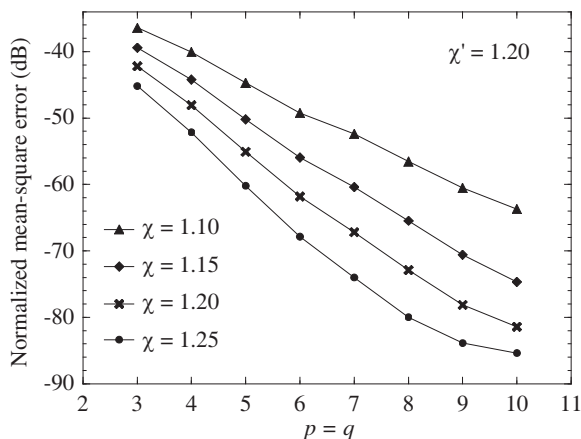


**Figure 13.** Normalized mean-square errors in the reconstruction of  $V$ .

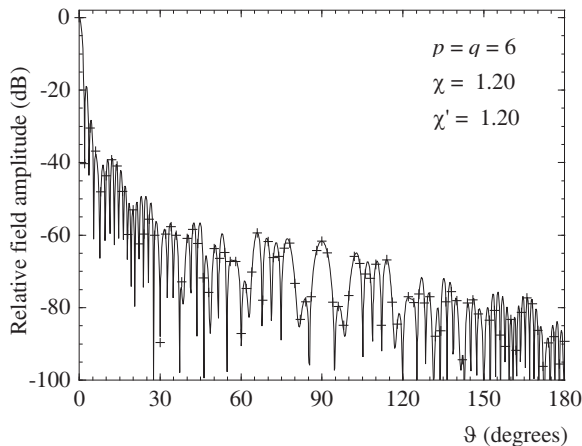


**Figure 14.**  $H$ -plane pattern. Solid line: Exact. Crosses: Reconstructed from NF measurements.

The reported numerical tests are relevant to a spiral lying on sphere of radius  $d = 35\lambda$  and to three uniform planar circular arrays placed at  $z = -4\lambda, 0\lambda, 4\lambda$ , having radius equal to  $16\lambda, 20\lambda$  and  $16\lambda$ , respectively. Their elements are elementary Huygens sources linearly polarized along  $y$  and are radially and azimuthally spaced by  $0.5\lambda$ . Such an antenna has been fitted by the described source modeling with  $c = c' = 4.5\lambda$  and  $a = 20\lambda$ , and again an open-ended circular waveguide, having radius  $\rho' = 0.338\lambda$ , has been considered as probe. Fig. 12 shows the reconstruction of the amplitude of the probe voltage  $V$  on the meridian at  $\varphi = 0^\circ$ . As can be seen, there is a very good agreement between the exact voltage and the reconstructed one. Note that we have adopted, in the zones of the spiral determined by the 46 samples around the poles, an excess bandwidth factor such that the sample spacing is reduced by a factor 11. The accuracy in the NF interpolation is also confirmed by the values of the mean-square errors (normalized to the voltage maximum value on the sphere) relevant to the probe voltage  $V$  and shown in Fig. 13 for  $p = q$  ranging from 3 to 10,  $\chi' = 1.20$ , and some  $\chi$  values. Also, in such a case, the algorithm has proved to be stable with respect to random errors affecting the NF data, but these results are not reported here for space saving. At last, the reconstruction of the FF pattern in the  $H$ -plane is shown in Fig. 14. As can be seen, the reconstruction is very accurate, thus assessing the effectiveness of the technique.

Note that the number of samples on the spiral is 28194, significantly less than the one (43 664) needed by the approach in [6]. In

particular, the number of “regular samples” at spacing  $\Delta\xi$  is 27 274, whereas the number of “extra samples” at reduced spacing is 920. Moreover, the number of samples collected along the spiral is much less than that (130 562) required by the NF-FF transformation with spherical scanning [9].

## REFERENCES

1. Special issue on near-field scanning techniques, *IEEE Trans. Antennas Propagat.*, Vol. 36, 727–901, June 1988.
2. Yaghjian, A. D., “An overview of near-field antenna measurements,” *IEEE Trans. Antennas Propagat.*, Vol. 34, 30–45, January 1986.
3. Yaccarino, R. G., L. I. Williams, and Y. Rahmat-Samii, “Linear spiral sampling for the bipolar planar antenna measurement technique,” *IEEE Trans. Antennas Propagat.*, Vol. 44, 1049–1051, July 1996.
4. Bucci, O. M., F. D’Agostino, C. Gennarelli, G. Riccio, and C. Savarese, “NF-FF transformation with spherical spiral scanning,” *IEEE Antennas Wireless Propagat. Lett.*, Vol. 2, 263–266, 2003.
5. D’Agostino, F., F. Ferrara, C. Gennarelli, G. Riccio, and C. Savarese, “Directivity computation by spherical spiral scanning in NF region,” *Journal Electromagnetic Waves and Applications*, Vol. 19, No. 10, 1343–1358, 2005.
6. D’Agostino, F., C. Gennarelli, G. Riccio, and C. Savarese, “Theoretical foundations of near-field-far-field transformations with spiral scannings,” *Progress In Electromagnetics Research*, Vol. 61, 193–214, 2006.
7. D’Agostino, F., F. Ferrara, C. Gennarelli, R. Guerriero, M. Migliozzi, and G. Riccio, “A nonredundant near-field to far-field transformation with spherical spiral scanning for nonspherical antennas,” *The Open Electrical & Electronic Eng. Jour.*, Vol. 3, 4–11, 2009.
8. Bucci, O. M., C. Gennarelli, and C. Savarese, “Representation of electromagnetic fields over arbitrary surfaces by a finite and nonredundant number of samples,” *IEEE Trans. Antennas Propagat.*, Vol. 46, 351–359, March 1998.
9. Hansen, J. E., Ed., *Spherical Near-field Antenna Measurements*, IEE Electromagnetic Waves Series, Peter Peregrinus, London, UK, 1998.

10. D'Agostino, F., F. Ferrara, C. Gennarelli, R. Guerriero, and M. Migliozi, "The unified theory of near-field-far-field transformations with spiral scannings for nonspherical antennas," *Progress In Electromagnetics Research B*, Vol. 14, 449–477, 2009.
11. Bucci, O. M., G. D'Elia, and M. D. Migliore, "Advanced field interpolation from plane-polar samples: Experimental verification," *IEEE Trans. Antennas Propagat.*, Vol. 46, 204–210, February 1998.
12. Bucci, O. M., F. D'Agostino, C. Gennarelli, G. Riccio, and C. Savarese, "Data reduction in the NF-FF transformation technique with spherical scanning," *Journal Electromagnetic Waves and Applications*, Vol. 15, No. 6, 755–775, 2001.
13. D'Agostino, F., F. Ferrara, C. Gennarelli, R. Guerriero, and M. Migliozi, "Effective antenna modelings for NF-FF transformations with spherical scanning using the minimum number of data," *International Journal of Antennas and Propagation*, No. 1687–5869, Article ID 936781, 2011.